High-performance Graphite||$Li_4Ti_5O_{12}$ Dual-ion Full Batteries Enabled by In-situ Formation of LiF-rich Solid Electrolyte Interphase on $Li_4Ti_5O_{12}$ Anode

Hekang Zhu[a], Shuyu Dong[a], Yu Zhao[a], Pui-Kit Lee[a], Denis Y. W. Yu[a,b *]

[a]School of Energy and Environment, City University of Hong Kong, Tat Chee Avenue, Kowloon, Hong Kong, P.R. China

[b]Research Center for Energy and Environmental Materials (GREEN), National Institute for Materials Science, Tsukuba, Ibaraki 305-0044, Japan.

E-mail: yu.denis@nims.go.jp (Denis Y. W. Yu)

Abstract

Dual-ion batteries (DIBs), well-known for the high-rate capability of the graphite cathode, urgently need a suitable anode material to realize their high power density in practical applications. In that respect, $Li_4Ti_5O_{12}$ (LTO), which can be cycled at high rates for thousands of cycles, can be a good candidate. However, a facile method to stabilize the graphite||LTO full cells is necessary. Herein, we introduce LiDFOB additive into the electrolyte of graphite||LTO cells, which drastically improves the cycling performance and reduces self-discharge of the DIBs. Specifically, by adding 1.0 wt.% LiDFOB to 2M $LiPF_6$ in fluorinated ethyl methyl carbonate, graphite||LTO DIBs can maintain stable charge-discharge for over 8000 cycles at 20 *C*. Characterizations indicate that LiDFOB forms a robust LiF-rich solid electrolyte interphase (SEI) on the LTO anode to suppress side reactions such as electrolyte decomposition and gas generation.

Key words: Dual-ion batteries; LiDFOB additive; graphite; $Li_4Ti_5O_{12}$; solid electrolyte interphase; LiF

Introduction

Dual-ion batteries (DIBs) with a low-cost graphite cathode have received much attention in recent years because of their high power output. The use of high-concentration electrolytes (HCE),[1]-[5] protective cathode electrolytes interface (CEI)[6]-[9] or surface coatings[10],[11] were able to suppress the degradation of the graphite cathode at high voltage, leading to superior performances with high rate charge/discharge and long cycling, which makes DIBs a competitive battery system for grid-scale energy storage stations.[12]-[17] However, the progress of DIBs for practical applications is slow primarily due to the lack of a matching anode. In particular, during fast charge, Li dendrite can easily form on the anode, jeopardizing the safety of the full cell.[18] In addition, the oxidative-resistant electrolytes that allow stable cycling of the graphite cathode above 5 V (*vs.* Li^+/Li) are usually not stable at the anode side.[19] To stabilize a DIB full cell, the common approach is to perform surface coating of the active materials or simultaneously constructing a cathode electrolyte interface/solid electrolyte interphase (CEI/SEI) layer on the cathode and anode, respectively. For instance, Li et al.[10] applied a Al_2O_3 coating to protect the graphite cathode and a 3D interphase film to suppress Li dendrite formation on the Li anode, which extended the stability of the graphite||Li cell to 2700 cycles. Wang et al.[9] used a mixed fluorinated ethylene carbonate/fluorinated ethyl methyl carbonate (FEC/FEMC) electrolyte to form protective CEI/SEI on both electrodes of a graphite||Li DIB, which can be cycled for over 5000 cycles. Nevertheless, the use of Li metal poses safety concerns due to its high reactivity and ease of Li dendrite formation. Thus, an alternative anode that can safely store cations is needed in a DIB full cell.

One of the issues of a DIB full cell is the mismatch of the cathode and anode caused by parasitic reactions, which is not obvious from the charge-discharge curves but can affect the electrochemical performances of the battery.[12] Specifically, in an ideal DIB, the same number of cations and anions in the electrolyte take part simultaneously in the charge-discharge process. However, if an electron-involving side reaction occurs in one of the electrodes, the opposite electrode will also have to compensate with an equal number of electrons. For example, the formation of an SEI layer on the surface of the anode will require extra anions to be inserted into the graphite cathode. On the other

hand, self-discharge with the de-intercalation of anions from the cathode due to side reactions at a high voltage can lead to an accumulation of cations at the anode, which causes a gradual shift in the state of charge of the anode.[12],[20],[21] Such issue is not a problem in half cells, for example, with Li metal anode where there is an abundant reservoir of Li, but can lead to significant cycle capacity decay in full cells.

There are a few studies to explore new anode materials for DIBs, such as silicon,[22] MoS_2,[23] Nb_2O_5,[24] microporous soft carbon,[25] porous aluminum foil,[26][27] Sn foil,[28] core-shell aluminum@carbon nanospheres,[29] Cu3P@P-doped carbon matrix,[30] carbon-coated $Fe_2P_4O_{12}$ anode,[31] small-molecule organic anode,[32] carbon-coated $MoS_{1.5}Te_{0.5}$ nano-cables,[33] Ti-doped niobium pentoxide nano-flakes,[34] carbon paper,[35] metastable Bi:Co and Bi:Fe alloys nano-dots@carbon.[36] Though, many of these works involve nano-materials that are not commercially available. In addition, most of the anodes have to be first pre-lithiated electrochemically before full cell assembly, which is not a practical method for commercial battery fabrication.

To extend the feasibility of graphite cathode for DIB, there are two requirements for the choice of anode in this study. First, it has to be capable of fast charge and discharge, and second, the anode should not need to be pre-lithiated. Among various anodes, $Li_4Ti_5O_{12}$ (LTO) is a good candidate. It has a stable potential plateau around 1.5 V (*vs.* Li^+/Li), far away from that for Li dendrite formation, and has already been proven to be a highly safe anode for Li-ion batteries (LIBs).[37] The robust spinel structure of LTO, which experiences near zero strain (~0.2%) during (de)lithiation,[38] enables long cycling stability of up to 117 000 cycles.[39] In addition, nano-crystal LTO was demonstrated to give high rate capability, e.g. over 100 mAh g^{-1} at 50 *C*.[40] However, stability of graphite||LTO DIBs is an issue to be solved.[41]-[44] For instance, the graphite||LTO DIBs demonstrated by Nozu et al. underwent severe electrolytes decomposition with the formation of a large amount of gas, resulting in poor cycle stability.[44] Interfacial reactions between LTO and electrolytes is a significant issue that needs to be suppressed.[41] Another difficulty is that high-voltage electrolytes that are compatible with the graphite cathode are often not suitable for the LTO anode.

Electrolyte additives, whose reduction potentials are higher than the potential plateau of LTO, such as vinylene carbonate (VC),[45] succinonitrile (SN),[46] methylene methanedisulfonate (MMDS)[47] and p-toluenesulfonyl isocyanate (PTSI),[48] were used to form a robust SEI and reduce gas generation on LTO for LIB. However, these additives may not be suitable for the high-voltage graphite cathode in DIBs. This study therefore aims to find an electrolyte additive that can be beneficial for both the LTO anode and the graphite cathode. In our previous works, lithium difluoro(oxalate)borate (LiDFOB) was shown to enhance the performances of the graphite cathode by forming a robust cathode electrolyte interface (CEI).[7],[8] In this work, we found that LiDFOB addition to ethyl methyl carbonate (EMC) or FEMC electrolyte can also drastically improve the electrochemical performances of graphite||LTO DIBs, demonstrating stable cycling to over 8000 cycles without any capacity fading with suppressed self-discharge. The change in state of charge of the cathode and anode during cycling and the surface of LTO was carefully examined to uncover the mechanism of the performance enhancement.

Experimental

Electrolytes and Electrodes – $LiPF_6$ (purity ≧ 99.95%) salt, EMC (purity ≧9 9.99%) and FEMC (purity ≧ 99%) solvents were purchased from Dongguan Shanshan Battery Materials Co. Ltd. and used without further purification. The base electrolytes are 3M $LiPF_6$ in EMC and 2M $LiPF_6$ in FEMC, which were optimized in our previous work to enable good performances in graphite||Li DIBs.[7]-[9] LiDFOB (Sigma Aldrich) additive is added to the base electrolytes in steps of 0.5 wt. % until saturation, where the maximum value is 2.5 wt. % in EMC and 1.0 wt. % in FEMC electrolytes. For simplicity, the base electrolytes are denoted as EMC and FEMC, and the electrolytes with the maximum amount of LiDFOB additive are denoted as EMC + LiDFOB and FEMC + LiDFOB.

The graphite (MTI SAG-R) cathode is composed of 85 wt. % active materials, 5 wt. % carbon black (Alfa, purity 99.9%, made from acetylene, 100% compressed) and 10 wt. % polyacrylic acid (PAA, Sigma-Aldrich, average Mv ~1,250,000, dissolved in

N-methyl-2-pyrrolidinone in advance with a ratio of 11 wt. %) binder on the Al foil. The anode is Li metal or LTO coated on Cu foil, with 70 wt. % nano-crystal LTO (Sigma-Aldrich), 19 wt. % carbon black (Alfa, purity 99.9%, made from acetylene, 100% compressed) and 1.0 wt. % single wall carbon nanotube (0.4 wt. %, dispersed in H_2O) as conductive additive, and 10 wt. % carboxymethyl cellulose sodium salt (CMC, Sigma-Aldrich, average Mv ~90,000) as binder. The electrodes were cut into circular discs (Φ15.6 mm for the cathode and Φ16.0 mm for the anode) after drying (80 ℃) in ambient atmosphere. The electrodes were further dried in vacuum in a Buchi oven (120 ℃) for 12 h before they were transferred into an Ar-filled glovebox (O_2 ≦ 0.1 ppm, H_2O ≦ 0.1 ppm). The mass loading of the active materials is 1.2 ± 0.2 mg cm^{-2} and 2.5 ± 0.2 mg cm^{-2} for the cathode and anode, respectively with excess amount of anode. Glass fiber filter (Advantec, GD-120) was used as the seperator and 200 uL electrolyte was added for each 2032-coin cell.

Electrochemical Tests and Characterizations – Galvanostatic charge-discharge was conducted to test the cycling stability at room temperature (22 ℃). All currents and capacities are calculated based on the mass of the graphite cathode. Graphite||Li half cells were cycled at 5 *C* (500 mAh g^{-1}) from 3.0 to 5.2 V, and the graphite||LTO full cells were cycled at 20 *C* (2000 mAh g^{-1}) after 2 cycles at 5 *C* from 2.0 to 3.7 V. To test the self-discharge performance of the batteries, graphite||LTO DIBs were charged at 1 *C* (100 mAh g^{-1}) to 3.6 V, rest for some time and then discharge to 2.0 V. The self-discharge of the graphite||Li half cells was also tested at 1 *C* by charging to 5.1 V.

The structures of the graphite and LTO were confirmed by XRD (X'Pert3 Powder X-ray Diffractometer, PANalytical) after cycling or charging. The surface compositions of the LTO after two cycles with Li counter electrode at 250 mA g_{LTO}^{-1} were examined by XPS (Thermo Scientific K-Alpha Nexsa) either at the pristine surface or with Ar^+ ions milling. All the spectra were calibrated according to the peak of C 1s at 248.8 eV. The cycled electrodes were obtained after disassembling the test cells and washed by dimethyl carbonate (DMC) before the characterization tests.

Results and Discussion

Cycling performance of graphite||LTO DIBs

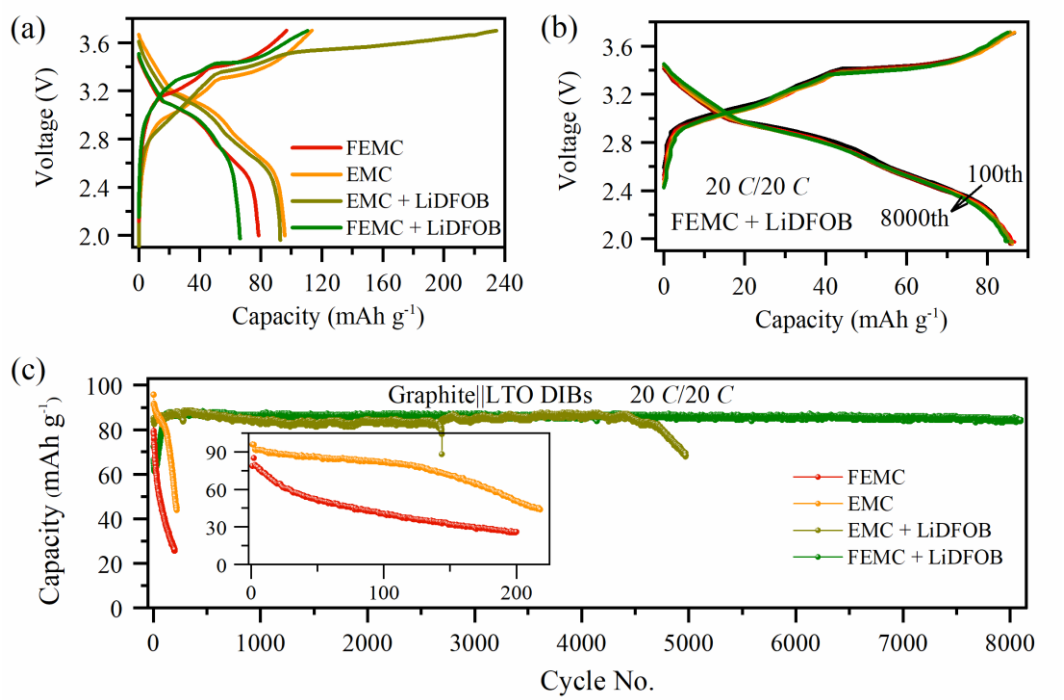

Figure 1. Electrochemical performances of graphite||LTO DIBs: (a) The first cycle voltage profiles, (b) selected voltage profiles of the 100th, 1000th, 2000th, 4000th, 6000th and 8000th cycle with FEMC + LiDFOB electrolyte; (c) cycling performance with FEMC, EMC, EMC + LiDFOB or FEMC + LiDFOB electrolytes. The inset figure in (c) shows the cycling performance for the first 200 cycles. Capacities are calculated based on the mass of the graphite in the cathode.

As-coated graphite cathode and LTO anode are assembled with different electrolytes into coin cells without pre-lithiating the LTO anode. The cells are first tested for 2 cycles at 5 *C*. The initial charge-discharge profiles of the full cells are shown in Figure 1a. The first charge and discharge capacities of the full cell with EMC are 113 and 95 mAh g^{-1}, respectively, with a first Coulombic efficiency (FCE) of 84%, indicating good reversibility of the graphite and LTO electrodes. When FEMC electrolyte is used, the available capacity is slightly lowered but FCE is still high (81%). The addition of LiDFOB additive into the EMC electrolyte leads to a larger initial charge capacity while the discharge capacity is about 92 mAh g^{-1}, which is attributed to the decomposition of LiDFOB at both the cathode and anode. The LiDFOB additive also increases the charge capacity in FEMC electrolyte and reduces the discharge

capacity from 81 to 66 mAh g^{-1} at the initial cycle, but the discharge capacity recovers to around 85 mAh g^{-1} after a few cycles (Figure 1c). The full cells are then subjected to cycling at 20 *C*. Charge-discharge curves of the full cells with cycling and the cycle performances are shown in Figure 1b, S1 and 1c. The full cell with FEMC electrolyte shows fast capacity fading to less than 40% of the initial capacity within 200 cycles. Similarly, the full cell with EMC electrolyte shows a fast capacity decline after 120 stable cycles. In comparison, cycle stability is significantly enhanced with the addition of LiDFOB. Stability is extended to more than 4500 cycles by adding LiDFOB to EMC electrolyte. The graphite||LTO cell with FEMC + LiDFOB can even maintain a stable capacity of 85 mAh g^{-1} with highly overlapping charge/discharge curves for 8000 cycles (Figure 1b). The Coulombic efficiency is around 100% during the long cycling after the initial 200 run-in cycles (Figure S2). Such superior cycling performance of the full graphite||LTO DIB has not been reported previously.

In order to understand the factors contributing to the cycle stability of the full DIBs, graphite||Li and LTO||Li half cells were tested in the different electrolytes. Interestingly, contrary to the fast capacity decline of graphite||LTO full cells, the cycling stability of the graphite and LTO half cells are extremely good in the FEMC or EMC electrolyte (Figure S3 and S4), with barely any capacity fading after cycling. LiDFOB additive shows minor effect on the performances of the half cells. The results suggest that the capacity decline of the full cell is not caused by the degradation of either the LTO anode or the graphite cathode but more likely by the mismatch of the cathode and the anode in the full cell due to losses of PF_6^- or Li^+ from side reactions.

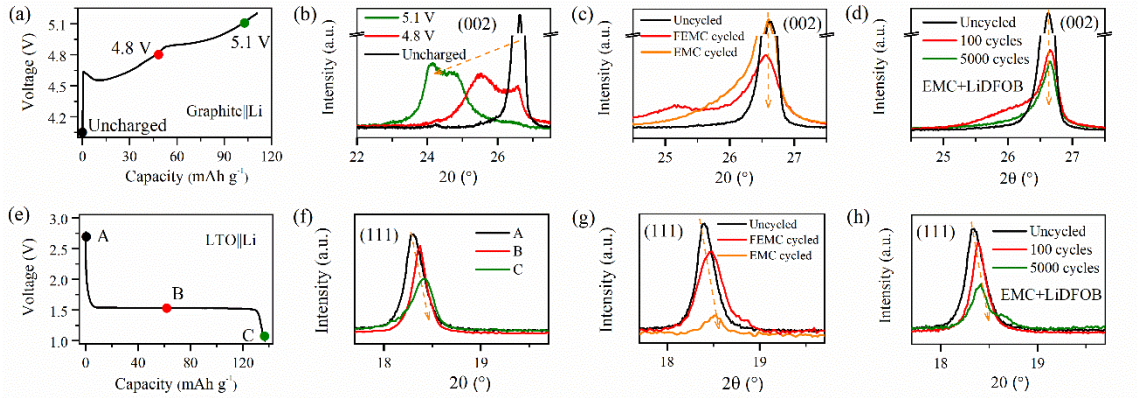

Figure 2. (a) The charged states of the graphite electrode and selected XRD (002) peaks

of the graphite electrode (b) at charged states of the half cell or (c,d) after cycling in graphite||LTO full cells. (e) The discharged states of the LTO electrode and selected XRD (111) peaks of the LTO electrode (f) at discharged states of the half cell or (g, h) after cycling of the full cells.

To explore the losses in graphite||LTO DIBs, we first study the structural changes of the graphite and LTO active materials during charge-discharge and cycling. Graphite||Li cells were first charged to 4.8 V and 5.1 V (as in Figure 2a) and they were disassembled for XRD measurements. As seen from Figure 2b, the graphite cathode expands in the *c* axis direction evidently when PF_6^- ions are inserted into the graphite layers,[43] as shown by the big shift of the (002) peak at 4.8 or 5.1 V (*vs.* Li^+/Li) compared to the uncharged state. The XRD peak shift therefore correlates with PF_6^- content in graphite. We then study the XRD peak shift of the graphite||LTO full cells. After 200 cycles in FEMC or EMC electrolyte, the (002) graphite peak position returns to that of the uncycled state. Similarly, after 100 cycles (without capacity decline) and 5000 cycles (capacity sharply declined) in EMC + LiDFOB electrolyte (Figure 2d), the (002) graphite peak position is still the same as pristine, indicating that PF_6^- ions are not accumulated inside the graphite cathode after cycling in the full cells.

Similarly, we investigate the structure change of LTO anode. LTO||Li half cells were first discharged to 60 mAh g^{-1} or 1.2 V and the LTO electrodes were taken out for XRD study (Figure 2e). With lithiation of LTO, a shift of the (111) peak of LTO to a higher diffraction angle with decreased peak intensity is observed (Figure 2f). The XRD peak shift also correlates with Li content in LTO. XRD of LTO extracted from graphite||LTO full cells in FEMC or EMC after 200 cycles shows that the structure of LTO is changed with cycling (Figure 2g). Comparing the LTO after 100 and 5000 cycles in EMC + LiDFOB electrolyte, there is a larger shift of the (111) peak to higher angle with larger decrease in peak intensity (Figure 2h). These results suggest that there is a gradual accumulation of Li^+ in the LTO with cycling in the full cell, which causes the poorer performance in graphite||LTO DIBs compared with graphite||Li DIBs.

Theoretically, in a DIB, the same number of cations and anions are inserted or removed from the anode and cathode, respectively during charge and discharge. The

gradual accumulation of cations inside the anode would indicate that there are parasitic oxidation reactions at the cathode that are consuming electrons but not PF_6^-.[12] This will cause a gradual imbalance of the two electrodes in the graphite||LTO full cell, leading to the observed capacity fading. Since the graphite||Li half cells show good cycle stability, we hypothesize that some of the reaction products originated from the LTO anode is transferred and oxidized at the cathode, and that the LiDFOB additive is able to reduce the side reactions at the LTO anode to improve the cycling performance. This will be further discussed in a later section.

Self-discharge of graphite||LTO DIBs

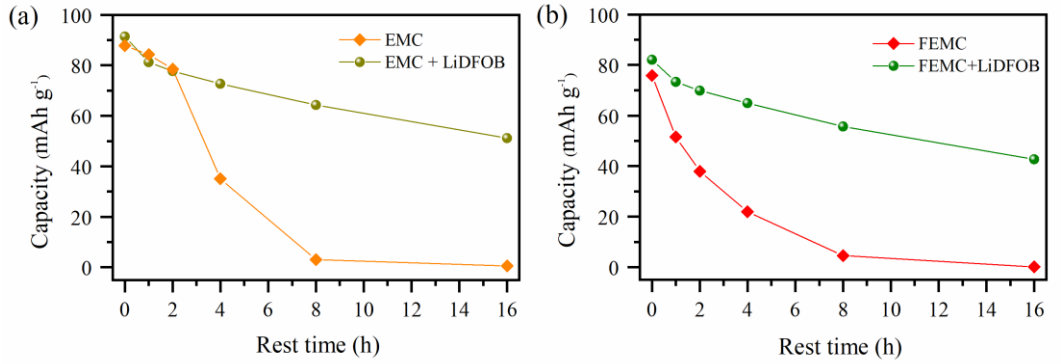

Figure 3. Self-discharge performance of graphite||LTO DIBs with electrolytes (a) EMC or EMC + LiDFOB, (b) FEMC or FEMC + LiDFOB.

Parasitic reactions on the electrodes could lead to self-discharge of the battery. To study it, we conduct a self-discharge test where we first fully charge the battery, rest for a certain number of hours, and then discharge. Self-discharge will lead to a drop in the obtained discharge capacity. The results for graphite||LTO are shown in Fig. 3. As the rest time is increased, the amount of capacity loss is also increased. One can see that the self-discharge of graphite||LTO is severe with EMC or FEMC electrolyte, where almost all the capacity is lost after 8 hours of rest. With the addition of LiDFOB into the electrolyte, the amount of self-discharge is reduced, indicating that LiDFOB is able to suppress some side reactions inside the full cell. A similar self-discharge test was also conducted on graphite||Li half cells (Figure S5). Here, we can see that regardless of whether the half cell is tested in EMC, FEMC with or without LiDFOB, the amount

of self-discharge capacity is the same. As the self-discharge tests of the graphite||LTO full cells is worse than that of graphite||Li half cells, one can conclude that same as the poor cycle stability, the increased self-discharge of the full cell is due to parasitic reactions brought by the LTO anode.

Effects of LiDFOB on SEI at LTO anode

We first explore the effect of LiDFOB on the graphite and LTO electrodes separately. Half cells of graphite||Li and LTO||Li with different electrolytes are prepared and tested, and the results are shown in Figure S6a and S6b. Since the addition of LiDFOB increases the initial charge capacity of the graphite||Li cell from around 100 mAh g^{-1} to over 150 mAh g^{-1} with an extended plateau at the end of charge, while it also increases the initial discharge capacity of LTO||Li cell from around 150 mAh g^{-1} to over 200 mAh g^{-1} with an extra higher potential discharge plateau at the starting stage, this indicates that LiDFOB is simultaneously oxidized at the graphite cathode and reduced at the LTO anode, which is attributed to the higher HOMO (the highest occupied molecular orbit) and lower LUMO (the lowest unoccupied molecular orbit) of LiDFOB compared to that of FEMC or EMC.[8],[49]-[51] This is consistent with the higher initial charge capacity of the graphite||LTO full cell with LiDFOB additive as shown in Figure 1a.

To further understand the effect of LiDFOB on the electrodes, graphite or LTO electrodes were first assembled with Li counter electrodes in EMC + LiDFOB or FEMC + LiDFOB electrolytes and cycled for 2 cycles. The electrodes, called “Cycled graphite” or “Cycled LTO”, are then taken out and re-assembled into full cells with fresh counter electrodes (i.e. Cycled graphite||LTO or graphite||Cycled LTO) in EMC or FEMC electrolyte without LiDFOB. The results are shown in Figure S6c and S6d. Note that for the Cycled graphite||LTO full cell, the initial available capacity is about 90 mAh g^{-1}, similar to that of the pristine graphite||LTO full cell. In addition, in EMC or FEMC electrolyte, the Cycled graphite||LTO full cells show fast capacity fading similar to the pristine graphite||LTO full cell. This indicates that the performance of the full cell is not affected by changes that the LiDFOB additive makes on the graphite cathode. In

comparison, the graphite||Cycled LTO shows better stability even when it is cycled in EMC or FEMC electrolyte without LiDFOB. This suggests that LiDFOB in the initial cell can stabilize the LTO electrode in future cycles even without LiDFOB.

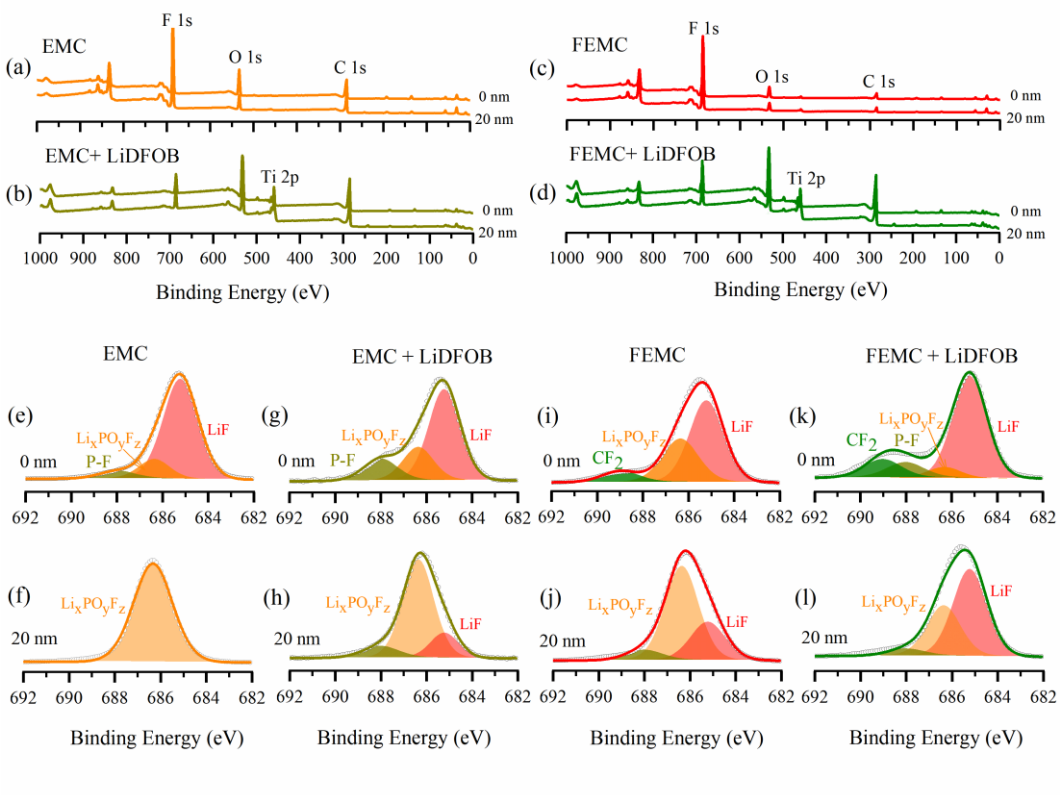

Figure 4. Full spectra and F 1s XPS profiles of the LTO electrodes in half cells with different electrolytes after 2 cycles: (a)(e)(f) EMC; (b)(g)(h) EMC + LiDFOB; (c)(i)(j) FEMC; (d)(k)(l) FEMC + LiDFOB. 0 nm refers to the spectra collected without ion milling; 20 nm refers to ion milling of 20 nm.

XPS was further adopted to uncover the effect of LiDFOB additive on the LTO surface. Figure 4a-4d show the XPS profile on the LTO surface. One can see peaks corresponding to only F, O and C in the SEI on the surface of the LTO that is cycled in EMC or FEMC (Figure 4a and 4c). Even with ion milling, Ti 2p peak cannot be observed, suggesting that the SEI layer is thick. In comparison, LTO cycled in EMC + LiDFOB or FEMC + LiDFOB shows more apparent Ti 2p signal with higher O 1s intensity (Figure 4b and 4d), which suggests that the LiDFOB additive enables a thinner SEI on the surface of LTO compared without it in the EMC or FEMC electrolytes.

F 1s XPS profiles of the LTO surface after cycling without or with ion milling are shown in Figure 4e to 4l. Even though the LTO surfaces in different electrolytes all

show LiF as the dominant species without ion milling (Figure 4e-4k), its amount differs through the surface layers (Figure 4f-4l). For LTO cycled in EMC, XPS peak corresponding to LiF disappears after ion milling (Figure 4f). The addition of LiDFOB to EMC electrolytes increases the LiF ratio in the SEI (Figure 4f and 4h). In comparison, larger amount of LiF is observed in the inner part of the SEI with FEMC electrolyte (Figure 4j), possibly from decomposition of FEMC. Combined with the contribution from the reduction of LiDFOB, the LTO surface cycled in FEMC + LiDFOB electrolyte shows the largest amount of LiF (Figure 4l). In addition to XPS, LiF signals are also observed in the XRD patterns of the cycled LTO electrodes (Figure S7), and the results are consistent with the XPS results. Since LiF is an electrical insulator, a LiF-rich SEI will block electron transfer on the surface, suppress the further decomposition of $LiPF_6$ and solvents, leading to a thinner SEI layer. Comparing FEMC, EMC, $LiPF_6$ and LiDFOB, LiDFOB has the lowest LUMO level, which suggests that LiDFOB has the highest priority to be reduced on the surface of the electrode (Figure 5a).[9],[51] Based on the above analysis, a possible mechanism is proposed for how the LiDFOB additive protects the LTO anode (Figure 5b). The thinner LiF-rich SEI layer initially formed with LiDFOB can stabilize the LTO surface, acting as an effective blocking layer to reduce decomposition of the electrolytes in future cycles.[51]-[53]

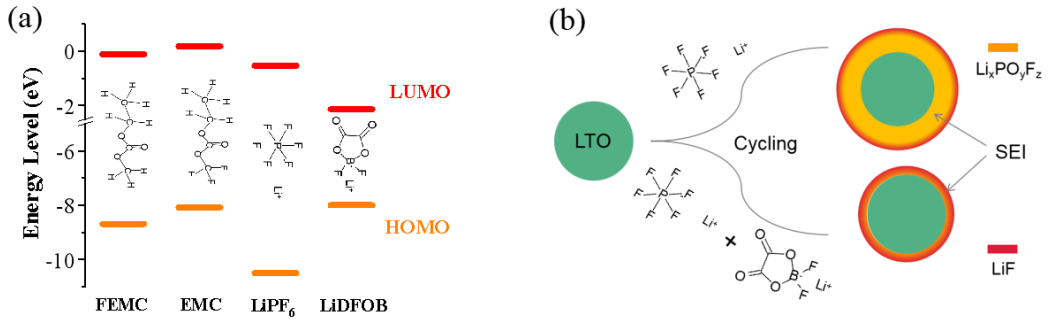

Figure 5. (a) LUMO and HOMO of FEMC, EMC, $LiPF_6$ and LiDFOB; (b) schematic of how LiDFOB additive affects the SEI on the LTO electrode.

We note that the coin cell of a graphite||LTO DIB tested in EMC electrolyte popped open after cycling (Figure S8), which would indicate that there is a buildup of gases inside such as H_2, CO and C_xH_y. generated from the reaction of LTO with carbonate

electrolytes.[41],[54] These gases can travel to the high voltage graphite cathode and be oxidized, resulting in an accumulation of Li^+ ions in the LTO anode, which well accounts for the unrecoverable states of LTO anodes after cycling (Figure 2g and 2h). The oxidation would also accelerate self-discharge of the graphite||LTO DIBs (Figure 3). The improved cycling and self-discharge performances with the LiDFOB additive suggest that the amount of by-product gases are reduced by the LiF-rich SEI on LTO, which can effectively block direct reaction between the LTO anode and the electrolyte.

To see how much LiDFOB additive is necessary, graphite||LTO DIBs were cycled in EMC or FEMC electrolyte with different amounts of LiDFOB (Figure S9 and Figure S10). One can see that the best cycle performance is achieved with the highest concentration of LiDFOB in both EMC and FEMC, i.e. 2.5 wt. % in EMC and 1.0 wt.% in FEMC. This is because a higher LiDFOB concentration can generate more reduction products and increase the LiF ratio in the SEI of LTO (Figure S9c). The best rate performance is also achieved with the highest concentration of LiDFOB (Figure S11). Comparing FEMC and EMC, our results show that 1.0 wt.% LiDFOB in 2M $LiPF_6$ FEMC electrolyte gives better cycle performance than 2.5 wt.% LiDFOB in 3M $LiPF_6$ EMC electrolyte. The use of FEMC and also the reduced amount $LiPF_6$ in the electrolyte is beneficial, as $LiPF_6$ can decompose on the LTO anode and worsen the performances.[51] Compared with other additives such as $TEABF_4$ or $LiBF_4$,[44],[55] LiDFOB can simultaneously form a protective layer on the graphite cathode and the LTO anode, which helps to enhance the cycle, rate, and self-discharge performances of the graphite||LTO dual-ion cells without sacrificing the discharge capacity.

Conclusions

In summary, we found the poor cycling performance of the graphite||LTO DIBs is due to the gradual accumulation of Li^+ in LTO electrode with cycling, which is not observed in graphite||Li with abundant amount of Li. Our results suggest that the gas generated from the LTO leads to parasitic reaction at the graphite cathode. By adding LiDFOB into the electrolyte, a thinner LiF-rich SEI layer is formed on the LTO anode, which suppresses the decomposition of electrolytes and reduces the amount of by-product

gases. As a result, cycling and self-discharge performances are significantly improved. This work not only introduces a high-efficient electrolyte (2M $LiPF_6$ in FEMC with 1.0 wt% LiDFOB) for graphite||LTO DIBs but also offers a strategy to suppress decomposition of electrolytes beyond their stable voltage windows.

Acknowledgement

This study was supported by a Research Matching Grant Scheme (PJ9229008) by the government of Hong Kong Special Administrative Region.

CRediT author statement

Hekang Zhu: Methodology, Formal analysis, Writing – original draft. **Shuyu Dong**: Investigation. **Yu Zhao**: Investigation. **Pui-Kit Lee**: Investigation. **Denis Y.W. Yu**: Funding acquisition, Supervision, Writing – review & editing.

Reference

[1]. K.V. Kravchyk, P. Bhauriyal, L. Piveteau, C.P. Guntlin, B. Pathak, M.V. Kovalenko, High-energy-density dual-ion battery for stationary storage of electricity using concentrated potassium fluorosulfonylimide, Nat. Commun. 9(1) (2018) 1-9.

[2]. L. Xiang, X. Ou, X. Wang, Z. Zhou, X. Li, Y. Tang, Highly concentrated electrolyte towards enhanced energy density and cycling life of dual-ion battery, Angew. Chem. Int. Ed. Engl. 59(41) (2020) 17924-17930.

[3]. X. Tong, X. Ou, N. Wu, H. Wang, J. Li, Y. Tang, High oxidation potential ≈6.0 V of concentrated electrolyte toward high-performance dual-ion battery, Adv. Energy Mater. 11(25) (2021) 2100151.

[4]. A. Heckmann, J. Thienenkamp, K. Beltrop, M. Winter, G. Brunklaus, T. Placke, Towards high-performance dual-graphite batteries using highly concentrated organic electrolytes, Electrochim. Acta 260 (2018) 514-525.

[5]. S. Miyoshi, H. Nagano, T. Fukuda, T. Kurihara, M. Watanabe, S. Ida, T. Ishihara, Dual-carbon battery using high concentration $LiPF_6$ in dimethyl carbonate (DMC) electrolyte, J. Electrochem. Soc. 163(7) (2016) A1206.

[6]. W.H. Li, Q.L. Ning, X.T. Xi, B.H. Hou, J.Z. Guo, Y. Yang, B. Chen, X.L. Wu, Highly improved cycling stability of anion de-/intercalation in the graphite cathode for dual-ion batteries, Adv. Mater. 31(4) (2019) 1804766.

[7]. Y. Wang, Y. Zhang, Q. Duan, P.-K. Lee, S. Wang, D.Y.W. Yu, Engineering cathode-electrolyte interface of graphite to enable ultra long-cycle and high-power dual-ion batteries, J. Power Sources 471 (2020) 228466.

[8]. Y. Wang, Y. Zhang, S. Wang, S. Dong, C. Dang, W. Hu, D.Y.W. Yu, Ultrafast Charging and Stable Cycling Dual-Ion Batteries Enabled via an Artificial Cathode-Electrolyte Interface, Adv. Funct. Mater. 31(29) (2021)

2102360.

[9]. Y. Wang, Y. Zhang, S. Dong, W. Zhou, P.K. Lee, Z. Peng, C. Dang, P.H.L. Sit, J. Guo, D.Y.W. Yu, An All-Fluorinated Electrolyte Toward High Voltage and Long Cycle Performance Dual-Ion Batteries, Adv. Energy Mater. (2022) 2103360.

[10]. W.H. Li, Y.M. Li, X.F. Liu, Z.Y. Gu, H.J. Liang, X.X. Zhao, J.Z. Guo, X.L. Wu, All-Climate and Ultrastable Dual-Ion Batteries with Long Life Achieved via Synergistic Enhancement of Cathode and Anode Interfaces, Adv. Func. Mater. 32(21) (2022) 2201038.

[11]. X. Han, G. Xu, Z. Zhang, X. Du, P. Han, X. Zhou, G. Cui, L. Chen, An in situ interface reinforcement strategy achieving long cycle performance of dual-ion batteries, Adv. Energy Mater. 9(16) (2019) 1804022.

[12]. T. Placke, A. Heckmann, R. Schmuch, P. Meister, K. Beltrop, M. Winter, Perspective on performance, cost, and technical challenges for practical dual-ion batteries, Joule 2(12) (2018) 2528-2550.

[13]. M. Wang, Y. Tang, A review on the features and progress of dual-ion batteries, Adv. Energy Mater. 8(19) (2018) 1703320.

[14]. X. Zhou, Q. Liu, C. Jiang, B. Ji, X. Ji, Y. Tang, H.M. Cheng, Strategies towards low-cost dual-ion batteries with high performance, Angew. Chem. Int. Ed. Engl. 59(10) (2020) 3802-3832.

[15]. G. Wang, M. Yu, X. Feng, Carbon materials for ion-intercalation involved rechargeable battery technologies, Chem. Soc. Rev. 50(4) (2021) 2388-2443.

[16]. C. Han, H. Wang, Z. Wang, X. Ou, Y. Tang, Solvation structure modulation of high-voltage electrolyte for high-performance K-based dual-graphite battery, Adv. Mater. 35(24) (2023) 2300917.

[17]. Y. Wei, B. Tang, X. Liang, F. Zhang, Y. Tang, Ultrahigh Mass-Loading Integrated Free-Standing Functional All-Carbon Positive Electrode Prepared Using Architecture Tailoring Strategy for High-Energy-Density Dual Ion Battery, Adv. Mater. (2023) 2302086.

[18]. J. Li, Z. Kong, X. Liu, B. Zheng, Q.H. Fan, E. Garratt, T. Schuelke, K. Wang, H. Xu, H. Jin, Strategies to anode protection in lithium metal battery: a review, InfoMat 3(12) (2021) 1333-1363.

[19]. L. Zhang, H. Wang, X. Zhang, Y. Tang, A review of emerging dual-ion batteries: fundamentals and recent advances, Adv. Func. Mater. 31(20) (2021) 2010958.

[20]. Z. Li, J. Liu, B. Niu, J. Li, F. Kang, A Novel Graphite-Graphite Dual Ion Battery Using an $AlCl_3$-[EMIm]Cl Liquid Electrolyte, Small 14(28) (2018) 1800745.

[21]. T. Placke, O. Fromm, S.F. Lux, P. Bieker, S. Rothermel, H.-W. Meyer, S. Passerini, M. Winter, Reversible intercalation of bis (trifluoromethanesulfonyl) imide anions from an ionic liquid electrolyte into graphite for high performance dual-ion cells, J. Electrochem. Soc. 159(11) (2012) A1755.

[22]. C. Jiang, L. Xiang, S. Miao, L. Shi, D. Xie, J. Yan, Z. Zheng, X. Zhang, Y. Tang, Flexible interface design for stress regulation of a silicon anode toward highly stable dual-ion batteries, Adv. Mater. 32(17) (2020) 1908470.

[23]. C. Cui, Z. Wei, J. Xu, Y. Zhang, S. Liu, H. Liu, M. Mao, S. Wang, J. Ma, S. Dou, Three-dimensional carbon frameworks enabling MoS_2 as anode for dual ion batteries with superior sodium storage properties, Energy Stor. Mater. 15 (2018) 22-30.

[24]. J. Zhu, Y. Xu, Y. Fu, D. Xiao, Y. Li, L. Liu, Y. Wang, Q. Zhang, J. Li, X. Yan, Hybrid aqueous/nonaqueous water-in-bisalt electrolyte enables safe dual ion batteries, Small 16(17) (2020) 1905838.

[25]. X. Yao, Y. Ke, W. Ren, X. Wang, F. Xiong, W. Yang, M. Qin, Q. Li, L. Mai, Defect-rich soft carbon porous nanosheets for fast and high-capacity sodium-ion storage, Adv. Energy Mater. 9(6) (2019) 1803260.

[26]. X. Tong, F. Zhang, B. Ji, M. Sheng, Y. Tang, Carbon-coated porous aluminum foil anode for high-rate, long-term cycling stability, and high energy density dual-ion batteries, Adv. Mater. 28(45) (2016) 9979-9985.

[27]. F. Zhang, B. Ji, X. Tong, M. Sheng, X. Zhang, C.S. Lee, Y. Tang, A dual-ion battery constructed with aluminum foil anode and mesocarbon microbead cathode via an alloying/intercalation process in an ionic liquid

electrolyte, Adv. Mater. Interfaces 3(23) (2016) 1600605.

[28]. M. Sheng, F. Zhang, B. Ji, X. Tong, Y. Tang, A novel tin-graphite dual-ion battery based on sodium-ion electrolyte with high energy density, Adv. Energy Mater. 7(7) (2017) 1601963.

[29]. X. Tong, F. Zhang, G. Chen, X. Liu, L. Gu, Y. Tang, Core-shell aluminum@ carbon nanospheres for dual-ion batteries with excellent cycling performance under high rates, Adv. Energy Mater. 8(6) (2018) 1701967.

[30]. X. Zhang, L. Zhang, W. Zhang, S. Xue, Y. Tang, A fast and stable sodium-based dual-ion battery achieved by Cu3P@ P-doped carbon matrix anode, J. Power Sources 518 (2022) 230741.

[31]. Z. Liang, D. Gong, J. Shang, H. Cheng, X. Pu, D. Wang, L. Zhang, C. Wang, C.-S. Lee, Y. Tang, Low volume expansion carbon-coated $Fe_2P_4O_{12}$ anode material for high-performance sodium dual-ion battery, Energy Stor. Mater. 53 (2022) 331-339.

[32]. X. Lei, Y. Zheng, F. Zhang, Y. Wang, Y. Tang, Highly stable magnesium-ion-based dual-ion batteries based on insoluble small-molecule organic anode material, Energy Stor. Mater. 30 (2020) 34-41.

[33]. Y. Liu, X. Hu, J. Li, G. Zhong, J. Yuan, H. Zhan, Y. Tang, Z. Wen, Carbon-coated $MoS_{1.5}Te_{0.5}$ nanocables for efficient sodium-ion storage in non-aqueous dual-ion batteries, Nat. Commun. 13(1) (2022) 663.

[34]. R. Yang, F. Zhang, X. Lei, Y. Zheng, G. Zhao, Y. Tang, C.-S. Lee, Pseudocapacitive Ti-doped niobium pentoxide nanoflake structure design for a fast kinetics anode toward a high-performance mg-ion-based dual-ion battery, ACS Appl. Mater. Interfaces 12(42) (2020) 47539-47547.

[35]. L.-N. Wu, Z.-R. Wang, P. Dai, Y.-X. Xie, C. Hou, W.-C. Zheng, F.-M. Han, L. Huang, W. Chen, S.-G. Sun, A novel high-energy-density lithium-free anode dual-ion battery and in situ revealing the interface structure evolution, Chem. Sci. 13(14) (2022) 4058-4069.

[36]. Z. Tong, T. Kang, Y. Wu, F. Zhang, Y. Tang, C.-S. Lee, Novel metastable Bi:Co and Bi:Fe alloys nanodots@ carbon as anodes for high rate K-ion batteries, Nano Research 15(8) (2022) 7220-7226.

[37]. H. Zhang, Y. Yang, H. Xu, L. Wang, X. Lu, X. He, $Li_4Ti_5O_{12}$ spinel anode: Fundamentals and advances in rechargeable batteries, InfoMat 4(4) (2022) e12228.

[38]. C. Han, Y.-B. He, M. Liu, B. Li, Q.-H. Yang, C.-P. Wong, F. Kang, A review of gassing behavior in $Li_4Ti_5O_{12}$-based lithium ion batteries, J. Mater. Chem. A 5(14) (2017) 6368-6381.

[39]. A. Jansen, A. Kahaian, K. Kepler, P. Nelson, K. Amine, D. Dees, D. Vissers, M. Thackeray, Development of a high-power lithium-ion battery, J. Power Sources 81 (1999) 902-905.

[40]. C. Wang, S. Wang, L. Tang, Y.-B. He, L. Gan, J. Li, H. Du, B. Li, Z. Lin, F. Kang, A robust strategy for crafting monodisperse $Li_4Ti_5O_{12}$ nanospheres as superior rate anode for lithium ion batteries, Nano Energy 21 (2016) 133-144.

[41]. T. Yuan, Z. Tan, C. Ma, J. Yang, Z.F. Ma, S. Zheng, Challenges of spinel $Li_4Ti_5O_{12}$ for lithium-ion battery industrial applications, Adv. Energy Mater. 7(12) (2017) 1601625.

[42]. X. Shi, S. Yu, T. Deng, W. Zhang, W. Zheng, Unlock the potential of $Li_4Ti_5O_{12}$ for high-voltage/long-cycling-life and high-safety batteries: Dual-ion architecture superior to lithium-ion storage, J. Energy Chem. 44 (2020) 13-18.

[43]. A. Yu, D. Gong, M. Zhang, Y. Tang, In-situ implanted carbon nanofilms into lithium titanate with 3D porous structure as fast kinetics anode for high-performance dual-ion battery, Chem. Eng. J. 401 (2020) 125834.

[44]. R. Nozu, E. Suzuki, O. Kimura, N. Onagi, T. Ishihara, Tetraethylammonium tetrafluoroborate additives for suppressed gas formation and increased cycle stability of dual-ion battery, Electrochim. Acta 337 (2020) 135711.

[45]. Y.-B. He, M. Liu, Z.-D. Huang, B. Zhang, Y. Yu, B. Li, F. Kang, J.-K. Kim, Effect of solid electrolyte interface (SEI) film on cyclic performance of $Li_4Ti_5O_{12}$ anodes for Li ion batteries, J. Power Sources 239 (2013) 269-276.

[46]. J. Gao, B. Gong, Q. Zhang, G. Wang, Y. Dai, W. Fan, Study of the surface reaction mechanism of $Li_4Ti_5O_{12}$ anode for lithium-ion cells, Ionics 21(9) (2015) 2409-2416.

[47]. R. Wang, X. Li, B. Zhang, Z. Wang, H. Guo, Effect of methylene methanedisulfonate as an additive on the cycling performance of spinel lithium titanate electrode, J. Alloys Compd. 648 (2015) 512-520.

[48]. R.-H. Wang, X.-H. Li, Z.-X. Wang, H.-J. Guo, Z.-J. He, Electrochemical analysis for enhancing interface layer of spinel $Li_4Ti_5O_{12}$: p-toluenesulfonyl isocyanate as electrolyte additive, ACS Appl. Mater. Interfaces 7(42) (2015) 23605-23614.

[49]. Q. Dong, F. Guo, Z. Cheng, Y. Mao, R. Huang, F. Li, H. Dong, Q. Zhang, W. Li, H. Chen, Insights into the dual role of lithium difluoro (oxalato) borate additive in improving the electrochemical performance of NMC811|| Graphite cells, ACS Appl. Energy Mater. 3(1) (2019) 695-704.

[50]. J. Chen, T. Liu, L. Gao, Y. Qian, Y. Liu, X. Kong, Tuning the solution structure of electrolyte for optimal solid-electrolyte-interphase formation in high-voltage lithium metal batteries, J. Energy Chem. 60 (2021) 178-185.

[51]. W. Shin, A. Manthiram, A Facile Potential Hold Method for Fostering an Inorganic Solid-Electrolyte Interphase for Anode-Free Lithium-Metal Batteries, Angew. Chem. Int. Ed. Engl. 61(13) (2022) e202115909.

[52]. L. Zhang, K. Zhang, Z. Shi, S. Zhang, LiF as an artificial SEI layer to enhance the high-temperature cycle performance of $Li_4Ti_5O_{12}$, Langmuir 33(42) (2017) 11164-11169.

[53]. Y. Zhang, Y. Luo, Y. Chen, T. Lu, L. Yan, X. Cui, J. Xie, Enhanced rate capability and low-temperature performance of Li4Ti5O12 anode material by facile surface fluorination, ACS Appl. Mater. Interfaces 9(20) (2017) 17145-17154.

[54]. M.S. Milien, J. Hoffmann, M. Payne, B.L. Lucht, Effect of electrolyte additives on $Li_4Ti_5O_{12}$ cycling performance and gas evolution, J. Electrochem. Soc. 165(16) (2018) A3925.

[55]. R. Nozu, E. Suzuki, O. Kimura, N. Onagi, T. Ishihara, Dual-ion battery using graphitic carbon and $Li_4Ti_5O_{12}$: Suppression of gas formation and increased cyclability, Electrochim. Acta 332 (2020) 135238.

TOC

LiDFOB additive forms a thin LiF-rich SEI on $Li_4Ti_5O_{12}$ (LTO) anode, successfully hinders the further decomposition of $LiPF_6$ and electrolyte. As a result, stable cycling of graphite||LTO dual-ion full batteries is extended to over 8,000 cycles.